Comparison of heat-transfer reduction in drag-reduced turbulent channel flows with different fluid and thermal boundary conditions

Takahiro Tsukahara*, Yasuo Kawaguchi

Department of Mechanical Engineering, Tokyo University of Science, 2641 Yamazaki, Noda-shi, Chiba 278-8510 Japan

Abstract

Direct numerical simulations of a drag-reduced viscoelastic turbulent channel flow with heat transfer were carried out for four kinds of rheologically different fluids, that is, with different values of Weissenberg number and viscosity ratio. The molecular Prandtl number was set to be 2.0. Two different thermal boundary conditions, namely, uniform heat flux heating and a constant temperature difference between two walls, were considered. We present the budget of temperature variance and investigation of the relationship between the heat-transfer reduction (HTR) and the drag reduction (DR) for each rheologically-different fluid. A case with a low viscosity ratio was found to give rise to high DR, with relatively low HTR compared with that obtained with a high Weissenberg number, suggesting dissimilarity between the heat and momentum transports.

Keywords: Channel flow; DNS; Drag reduction; Giesekus model; Non-Newtonian fluid; Rheology; Similarity of heat and momentum; Toms effect; Turbulence control; Turbulent heat transfer; Viscoelastic fluid.

*Corresponding author
Email address: tsuka@rs.tus.ac.jp (Takahiro Tsukahara)

Please cite this article as: Tsukahara, T., et al. Comparison of heat-transfer reduction in drag-reduced turbulent channel flows with different fluid and thermal boundary conditions. Progress in Computational Fluid Dynamics, Vol. 11 (2011), 215–225. doi:10.1504/PCFD.2011.041022

1. Introduction

The addition of small amounts of long-chain polymer molecules or surfactant additives to wall-bounded turbulent flows can lead to a dramatic drag reduction (DR). This effect is known as 'Toms Effect' since Toms (1948) discovered this phenomenon. The application of this phenomenon to heat-transport systems such as district heating and cooling systems has attracted attention recently as an energy-saving technology. The pumping power can be largely conserved by adding a few hundred ppm of surfactant solution to water so that the flow becomes laminar-like. On the other hand, a heat-transfer reduction (HTR) for a drag-reduced flow also becomes significantly large with an increase in the drag reduction rate. If we can find a kind of fluid that gives rise to 'large' DR and 'small' HTR, it could be a suitable transporter of heat in thermal systems.

The reduction in drag in turbulent flow due to additives has been investigated by many researchers through direct numerical simulation (DNS) and experiment (e.g., Sureshkumar et al., 1997; Dimitropoulos et al., 2001; Li and Kawaguchi, 2004; Yu and Kawaguchi, 2004; Jovanović et al., 2006; White and Mungal, 2008). However, although research on drag-reducing flow with heat transfer is important for the above-mentioned heat-transport systems and interesting from a scientific perspective, there have been very few studies on this issue (Dimant and Poreh, 1976; Li and Kawaguchi, 2004; Li et al., 2005; Gasljevic et al., 2007), particularly in terms of numerical simulations. Yu and Kawaguchi (2005) carried out DNS at a friction Reynolds number of $Re_\tau = 150$ and a Prandtl number of $Pr = 0.71$ for uniform wall heat flux heating (UHF), and Kagawa et al. (2008) undertook studied at a higher Prandtl number of $Pr = 2$. However, to the best of our knowledge, no studies on a drag-reducing flow for a thermal boundary condition other than UHF have been undertaken; that is, for a constant temperature difference (CTD) between top and bottom walls. As is well known, in spite of its geometrical simplicity, the combination of factors (i.e., Re, Pr, and thermal boundary condition) causes a large variation in the turbulent heat transfer of channel flow. The present study, considering two thermal boundary conditions, is important to investigate the dissimilarity between the velocity and temperature fields and is motivated by the need for a turbulence model for turbulent scalar fluxes.

In this study, we carried out a series of DNS on turbulent heat transfer in a drag-reduced channel flow at $Re_\tau = 150$ and $Pr = 2.0$ using a Giesekus

model. Moreover, UHF and CTD were employed as the thermal boundary conditions. The temperature is considered as a passive scalar. We observed that there were different drag-reducing mechanisms at the same level of drag reduction rate ($DR\%$) for rheologically different fluids. Thus, we focus on the relationship between the drag reduction and the heat-transfer reduction rate.

2. Numerical procedures

The turbulent flow that we considered in this study was assumed to be fully developed along the x direction, in a plane channel of height $L_y = 2\delta$, as shown in Figure 1, in which x, y, and z are the streamwise, wall-normal, and spanwise directions, respectively. The periodic boundary condition was adopted in the horizontal (x and z) directions, and the non-slip boundary condition was imposed on the walls. All present DNS were run under a constant pressure drop, so the friction Reynolds number was fixed at a constant of $Re_{\tau 0} = 150$ (defined below).

The dimensionless governing equations for an incompressible viscoelastic-fluid flow, namely, for the velocity vector $u_i = \{u, v, w\}$, the pressure p, and the conformation tensor c_{ij}, are the continuity, momentum, and constitutive equations based on Giesekus model as follows:

$$\frac{\partial u_i}{\partial x_i} = 0, \tag{1}$$

$$\begin{aligned}\frac{\partial u_i^+}{\partial t^*} + u_j^+ \frac{\partial u_i^+}{\partial x_j^*} &= -\frac{\partial p^+}{\partial x_i^*} + \frac{\beta}{Re_{\tau 0}} \frac{\partial}{\partial x_j^*} \left(\frac{\partial u_i^+}{\partial x_j^*} \right) \\ &\quad + \frac{(1-\beta)}{We_\tau} \frac{\partial c_{ij}^+}{\partial x_j^*} + \frac{\partial \overline{p}^+}{\partial x_1^*} \delta_{1i},\end{aligned} \tag{2}$$

$$\begin{aligned}\frac{\partial c_{ij}^+}{\partial t^*} + \frac{\partial u_k^+ c_{ij}^+}{\partial x_k^*} &= \frac{\partial u_i^+}{\partial x_k^*} c_{kj}^+ + \frac{\partial u_j^+}{\partial x_k^*} c_{ki}^+ \\ &\quad - \frac{Re_{\tau 0}}{We_\tau} \left[c_{ij}^+ - \delta_{ij} + \alpha \left(c_{ik}^+ - \delta_{ik} \right) \left(c_{kj}^+ - \delta_{kj} \right) \right],\end{aligned} \tag{3}$$

where t is the time, δ_{ij} the Kronecker delta, and α the mobility factor. As suggested by Equation (2), the flow is defined by three control parameters

of:

$$\text{Friction Reynolds number:} \qquad Re_{\tau 0} = \frac{u_\tau \delta}{\eta_0}, \tag{4}$$

$$\text{Weissenberg number:} \qquad We_\tau = \frac{\lambda}{\eta_0 / u_\tau^2}, \tag{5}$$

$$\text{Viscosity ratio:} \qquad \beta = \frac{\eta_\mathrm{s}}{\eta_0}, \tag{6}$$

where u_τ is the friction velocity representative of the total drag of the wall surfaces, λ the relaxation time, η_0 the zero-shear-rate kinematic viscosity, and η_s the kinematic viscosity of the Newtonian solvent. In Equations (1)–(3), the superscripts of * and $^+$ represent non-dimensionalization with δ and that by u_τ and ν, respectively. Equation (3) is derived on the basis of Giesekus model for a viscoelastic fluid, in order to calculate the extra stress, τ_{ij}, caused by the interaction between shear rate and the fluid elasticity due to additives. The dimensionless conformation tensor, c_{ij}^*, in Equations (2) and (3) is given as follows:

$$\tau_{ij}^+ = \frac{c_{ij}^+ - \delta_{ij}}{\lambda u_\tau / \delta}. \tag{7}$$

Note that, in general, both λ and η_0 can be considered as functions of the stress or other state variables (e.g., temperature), but they will be assumed to be constants in this study for simplicity.

With the calculated flow field, the temperature $T(x, y, z)$ was obtained by integrating the equation of energy conservation:

$$\frac{\partial T^+}{\partial t^*} + u_j^+ \frac{\partial T^+}{\partial x_j^*} = \frac{1}{Re_{\tau 0} Pr} \frac{\partial^2 T^+}{\partial x_j^{*2}}, \tag{8}$$

with non-dimensionalization by the friction temperature. The thermal boundary condition, either UHF or CTD, was imposed as illustrated in Figure 1. For UHF, both walls are uniformly heated with constant wall heat flux (but the instantaneous heat flux is time-dependent), so that the statistically averaged temperature increases linearly with respect to the x direction. Therefore, the transformed temperature, $\theta(x, y, z)$, is introduced from the following equation:

$$T(x, y, z) = \frac{\mathrm{d}T_\mathrm{m}}{\mathrm{d}x} x - \theta(x, y, z), \tag{9}$$

where T_m is the bulk mean temperature defined as follows:

$$T_\mathrm{m} = \frac{\int_0^\delta \overline{u}\,\langle T\rangle\,\mathrm{d}y}{\int_0^\delta \overline{u}\mathrm{d}y}. \tag{10}$$

Here, $\langle T\rangle$ is the temperature averaged in time and in the z direction, while an overbar denotes a quantity also averaged in the x direction. The denominator of Equation (10) corresponds to the bulk mean velocity, $u_\mathrm{m} = \int_0^1 \overline{u}\mathrm{d}y^*$. From the heat flux balance and the present configuration, the streamwise temperature gradient in Equation (9) becomes

$$\frac{\mathrm{d}T_\mathrm{m}^+}{\mathrm{d}x^*} = \frac{1}{u_\mathrm{m}^+}. \tag{11}$$

In the case of CTD, the instantaneous temperature of $T\,(x,y,z)$ can be divided into two terms as follows:

$$T\,(x,y,z) = \frac{\Delta T}{2\delta}y + \theta\,(x,y,z)\,. \tag{12}$$

Then, we can arrange the equation for $\theta\,(x,y,z)$ from Equation (8) into the following form, for each thermal boundary condition.

$$\frac{\partial\theta^+}{\partial t^*} + u_j^+\frac{\partial\theta^+}{\partial x_j^*} = \frac{1}{Re_{\tau 0}Pr}\frac{\partial^2\theta^+}{\partial x_j^{*2}} + \Theta, \tag{13}$$

$$\Theta = \begin{cases} \dfrac{u}{u_\mathrm{m}} & \text{for UHF} \\ -\dfrac{\Delta T^+}{2}v^+ & \text{for CTD.} \end{cases} \tag{14}$$

Since the present simulations are continuations of the DNS without passive scalar transport, as reported by Yu and Kawaguchi (2004), the numerical procedure is briefly described as follows. For the spatial discretization, the finite difference method was adopted, but the pressure Poisson equation was solved in Fourier space. A numerical scheme with fourth-order accuracy was employed in the x and z directions, and that with second-order accuracy was applied in y. The first/second-order MINMOD scheme was adapted to the convective term in Equation (3). This scheme is a composite flux-limiter scheme (almost identical to the SOUCUP scheme) consisting of the second-order upwind, central differencing, and first-order upwind schemes (see Zhu

and Rodi, 1991; Yu and Kawaguchi, 2004). Time advancement was carried out by the second-order Adams-Bashforth method, but the Crank-Nicolson method was for the viscous terms in the wall-normal direction.

In the present work, we investigated the reduction rates of the drag and the heat transfer for different thermal boundary conditions and their dependences on the fluid rheological parameters of the Weissenberg number We_τ and the viscosity ratio β. It was expected that the rate of heat-transfer reduction would be an increasing function of Weissenberg number—indeed, the results of the simulations support this supposition. Therefore, we tested a low Weissenberg number for examination with modestly modulated velocity/thermal fields, in addition to high values giving rise to a nearly maximum drag reduction. Table 1 shows a summary of parameters for the Newtonian fluid (Case 1) and the viscoelastic fluids (Case 2–4). As can be seen from the table, a comparison between Cases 3a and 3b is equivalent to examining the effect of a decrease of β with a fixed We_τ, while the condition change among Cases 2, 3a, and 4 is variation in We_τ at constant β. The other fluid properties of $\alpha = 0.001$ and $Pr = 2.0$ were assumed to be dependent on neither the flow nor the temperature fields.

The dimensions of the computational domain are $12.8\delta \times 2\delta \times 6.4\delta$ in the x, y, and z directions, being discretized into $128 \times 128 \times 128$ grid points. The dimensionless grid resolutions in the x and z directions are evenly distributed ($\Delta x = 0.1$, $\Delta z = 0.05$). In the wall-normal direction, the resolutions are stretched away from the walls, in which Δy ranges from 0.0015 at the walls to 0.030 at the channel center. In this study, the friction Reynolds number is set as 150. The dimensionless element sizes in wall units, Δx^+,Δy^+, and Δz^+, are 15.0, 0.226–4.52, and 7.5, respectively. The spatial resolution employed in the current DNS is comparable to those in previous studies (Kagawa et al., 2008; Tsukahara et al., 2011). The dimensionless time incremental interval, Δt^+, is 1.5×10^{-3}.

3. Result and discussion

3.1. Velocity field in drag-reduced turbulence

Firstly, we shall briefly discuss the flow (velocity) field accompanied by the wall-turbulence modulation and the drag reduction due to the fluid viscoelasticity, prior to any consideration of the passive-scalar (temperature) field.

The mean-velocity profile, $\overline{u}^+$, in wall-unit coordinate is shown in Figure 2, where the experimental data of Yu et al. (2004) are also presented. Note again that statistics are denoted by an overbar, which are the spatially (in x and z) and temporally averaged. It should also be noted that we use $y_\eta = yu_\tau/\eta_{\text{eff}}$ in the abscissa axis, where η_{eff} is effective wall kinematic viscosity calculated from the proportionality between the total wall shear stress $\tau_w = \rho u_\tau^2$ and the mean velocity gradient at the wall as follows:

$$\left|\frac{\tau_w}{\rho}\right| = \eta_{\text{eff}} \left|\frac{\mathrm{d}\overline{u}}{\mathrm{d}y}\right|_{y=0}. \tag{15}$$

In a Newtonian flow, $\eta_{\text{eff}} = \eta_0$ and thus $y_\eta = y^+$. By applying this normalization, velocity profiles in the drag-reduced turbulent channel flow are scaled well, as given in the figure.

Onset of drag reduction is observed in all cases of viscoelastic fluid (Cases 2–4), being accompanied by an upward shift of the log-law velocity profile (see Figure 2). In sharp contrast to the Newtonian flow (Case 1), there is an elastic layer between the viscous sublayer and the log-law region in the drag-reduced viscoelastic flow, in which the velocity profile is in accordance with the maximum drag-reduction asymptote (MDRA) proposed by Virk (1971). It is known that a shift of the logarithmic law occurs in drag-reduced wall turbulence and the magnitude of the shift is related to the drag-reduction rate (Lumley, 1969; Gyr and Bewersdorff, 1995). With increasing We_τ, the shift magnitude increases until MDRA is approached at $We_\tau = 40$; in Case 4, a log-law region no longer appears between the elastic layer and the core region. Similar behavior was seen in the experimental results (Yu et al., 2004). In such a case, the turbulent diffusion is suppressed because small turbulent eddies are dampened. However, the log-law profile for the other viscoelastic flows can be observed from a position higher than that of Case 1. If we consider the different viscosity ratio β at the same Weissenberg number, a difference in the outer layer between Cases 3a and 3b is also apparent. Although the shift magnitude in Case 3b is larger than that in Case 3a, the existence of a log-law region implies a wide range of turbulent-eddy scales in the flow. Therefore, the turbulent contribution to the momentum transfer is not so different between them, but the further upward shifting in the log-law region of Case 3b is attributed to a decrease of the effective viscosity, as shown later in Table 2, by decreasing β.

These trends, that is, the two aspects of the coupling between fluid rheol-

ogy and amount of drag reduction, have already been identified and discussed in detail in Ishigami et al. (2009) and Tsukahara et al. (2011). The first aspect is the reduced contribution of turbulence due to a high We_τ, and the second one is the decreased effective viscosity by a low β. Through these aspects, the drag reduction should be enhanced. In the following sections, we analyze whether the temperature field, as well as the reduction in heat-transfer rate, undergoes different modulation depending on these aspects.

3.2. Variation in mean temperature profile

Figure 3 shows the dimensionless mean temperature profile for both UHF and CTD. Similar to that of $\overline{u}$, the vertical profile of $\overline{\theta}$ in UHF is symmetric about the channel center. On the other hand, for CTD, the mean temperature gradient exists even in the core region, revealing a considerable difference for the two thermal boundary conditions. For instance, Case 4 has a steep gradient at the channel center. It was caused by the turbulence suppression at high We_τ. The profiles for both conditions seem to approach each laminar heat-transfer solution with increasing We_τ. The profile in Case 3b is almost coincident with (or slightly lower than) that in Case 3a, although a difference in the mean velocity profile is noticeable in the outer layer (see Figure 2). This is due to the heat-conductive sublayer being thinner in Case 3b, as well as the narrow viscous sublayer due to the reduced effective viscosity.

To compare with the mean velocity profile, the mean temperature nondimensionalized by the friction temperature is plotted in wall unit, as given in Figure 4. Note that the wall-normal distance y as the abscissa is nondimensionalized by η_0, not by η_{eff}. For UHF, the result of Case 1 is in good agreement with the DNS data of Kozuka et al. (2009), who performed a high-resolution DNS at high Prandtl numbers up to 10. The linear relationship of $\theta^+ = Pr \cdot y^+$ in the conductive sublayer disappeared at $y^+ \approx 5$ for all cases. From the buffer layer of $y^+ > 5$, Weissenberg-number dependence was clearly observed. The log-law region of viscoelastic fluids shifted up from that of Newtonian fluid, but the layer could not be observed clearly in Case 4, similar to the mean velocity profile. Also shown in the figure is a fitting curve $(c_1 \ln y^+ + c_2)$ for a log region in Case 4, which can be appropriate for both thermal conditions. However, it is obvious from the figure that its coefficients of c_1 and c_2 are not universal values, but instead depend on the Weissenberg number.

3.3. Reduction rates of drag and heat transfer

Table 2 shows the mean flow variables, such as the bulk Reynolds number $Re_{\mathrm{m}} = 2u_{\mathrm{m}}\delta/\eta_0$, the ratio of the fluid kinematic viscosity η_0 to the effective value η_{eff}, and the reduction rates of drag and heat transfer. The drag and heat-transfer reduction rates are evaluated by the following equations:

$$DR\% = \frac{C_{f\,\mathrm{Newt}} - C_{f\,\mathrm{visc}}}{C_{f\,\mathrm{Newt}}}, \tag{16}$$

$$HTR\% = \frac{Nu_{\mathrm{Newt}} - Nu_{\mathrm{visc}}}{Nu_{\mathrm{Newt}}}, \tag{17}$$

where $C_{f\,\mathrm{visc}}$ and Nu_{visc} are, respectively, the friction coefficient and the Nusselt number obtained by the present DNS for viscoelastic fluids. The subscript 'Newt' represents those for Newtonian-fluid flow at the same value of Re_{m}, estimated from the following empirical correlation function based on existing works (Dean, 1978; Kays and Crawford, 1980; Tsukahara et al., 2006):

$$C_{f\,\mathrm{Newt}} = 0.073 Re_{\mathrm{m}}^{-0.25}, \tag{18}$$

$$Nu_{\mathrm{Newt}} = 0.020 Re_{\mathrm{m}}^{0.8} Pr^{0.5} \quad \text{for UHF}, \tag{19}$$

$$Nu_{\mathrm{Newt}} = 0.016 Re_{\mathrm{m}}^{0.8} Pr^{0.5} \quad \text{for CTD}. \tag{20}$$

Although the function of Kays and Crawford (1980) is applicable only for UHF, the DNS database obtained by Tsukahara et al. (2006) revealed the same tendency for CTD, that is an increase of Nu_{Newt} in proportion to $Re_{\mathrm{m}}^{0.8}$, at least in the range of $110 \leq Re_{\tau 0} \leq 180$.

As mentioned in Section 3.1, there are two aspects causing the DR in the viscoelastic turbulent flow. One is the suppression of turbulent production under a high-We_τ condition, and the other is the diminution in the effective viscosity (decrease of η_{eff}) with a low-β condition. Indeed, the conditions in which a high $DR\%$ was achieved in the range of the present study were Case 4 (a high-We_τ fluid) and Case 3b (a low-β fluid). Therefore, the HTR in these cases were also enhanced, resulting in high $HTR\%$. In Case 3a, slightly lower but still significant $DR\%$ and $HTR\%$ were obtained. These values increased by about 9%, as We_τ changed from 30 to 40. When β is decreased at a constant We_τ, $HTR\%$ increases slightly and the ratio of $\eta_0/\eta_{\mathrm{eff}}$ is also increased.

From comparison of the different boundary conditions, a clear difference in $HTR\%$ cannot be observed: the highest $HTR\%$ flow is in Case 4. The

ratio of $HTR\%/DR\%$ is also shown in Table 2. In each case, $HTR\%$ for CTD is 3–5% larger than that for UHF and also slightly exceeds the magnitude of $DR\%$—the ratio is more than 1— except for Case 2. As mentioned in the introduction, a low value of the ratio of $HTR\%/DR\%$ is desirable for engineering applications, for instance, a heat exchanger. According to the results, the fluid condition in Case 2 might be adequate to avoid the attenuation of turbulent heat transfer. However, we focus mainly on the highly drag-reduced turbulent flows, that is, Cases 3a, 3b, and 4, since a study of such modulated turbulence is practically required.

The relationships between the Nusselt number Nu and the bulk Reynolds number Re_{m} for all cases are plotted in Figure 5. The relationships in Case 1 of both conditions agree well with each empirical correlation for the turbulent regime of a Newtonian fluid. It can be clearly seen that, for the other cases, Nu becomes lower as Re_{m} increases; Nu is roughly invesely proportional to Re_{m}. However, the obtained Nu in Case 3b is significantly deviated from the fitting curve. Therefore, it is conjectured that the decrease of β gives rise to large $DR\%$ with relatively small $HTR\%$ compared with the results with increasing We_τ. The values of Nu for CTD were smaller than those for UHF, but similar trends were seen for the two thermal conditions.

3.4. Temperature variance

The temperature variance $\theta'^{+}_{\mathrm{rms}}$, that is, root-mean-square (RMS) of temperature fluctuations, normalized by the friction temperature, is shown in Figure 6, where the distributions for UHF and CTD are shown in (a) and (b), respectively. In both UHF and CTD, it can be seen that $\theta'^{+}_{\mathrm{rms}}$ increases more at higher $DR\%$ throughout the channel and that the near-wall peak shifts away from the wall as the Weissenberg number changes from $We_\tau = 0$ to 40. When We_τ is fixed, the $\theta'^{+}_{\mathrm{rms}}$-distribution as well as its peak position does not exhibit a significant variation with β. In the case of CTD, it was observed that a secondary peak arose at the channel center for all present conditions, as shown in Figure 6(b). In Case 4 in particular, this secondary peak is larger than that of the near-wall region. This is attributed to the steep temperature gradient at the channel central region, which is more prominent at higher $DR\%$ (see Figure 3). In highly drag-reduced turbulent flow, the heat transport by near-wall turbulence is expected to be dampened and thus the bulk mean temperature for CTD becomes markedly different between the top and bottom halves of the channel.

It can be seen from Figure 6 that, in Case 2, the value of $\theta'^{+}_{\mathrm{rms}}$ in the buffer region ($5 < y^{+} < 70$) is slightly larger than for the Newtonian flow of Case 1, implying that the influence of the turbulence modulation due to the fluid viscoelasticity occurs there and does not exist in the core region ($70 < y^{+}$). Although the attenuation of the momentum and heat transports in Case 2 seems to be small and limited in the near-wall region, non-negligible $DR\%$ and $HTR\%$ are obtained, as given in Table 2. This is because the turbulent heat flux as well as the Reynolds shear stress in the near-wall region should primarily contribute to the heat transfer and the frictional drag, in the context of the FIK identity (see Fukagata et al., 2002; Kagawa et al., 2008). The turbulence contribution in the Nusselt number can be described explicitly as follows:

$$Nu = \int_0^1 (1 - y^*) \left(-\overline{v'^{+}\theta'^{+}}\right) \mathrm{d}y^* + \mathrm{o.c.} \tag{21}$$

for the configuration we consider in the present study. Here, 'o.c.' means other contributions, such as the viscous contribution. Therefore, the wall-normal turbulent heat flux, contained in the component shown in Equation (21), will be discussed below.

3.5. Wall-normal turbulent heat flux

The turbulent heat flux in the wall-normal direction, normalized by u_τ and the friction temperature, is plotted in Figures 7(a) and 7(b) for UHF and CTD, respectively. For comparison purposes, the high-resolution DNS result of UHF in a Newtonian flow obtained by Kozuka et al. (2009) (for $Pr = 2$, $Re_\tau = 180$) is included. The present DNS of the Newtonian flow is in reasonable agreement with their result and the maximum of $-\overline{v'^{+}\theta'^{+}}$ is also located at $y^{+} \approx 26$. In the viscoelastic flow, $-\overline{v'^{+}\theta'^{+}}$ is depressed in the near-wall region, but almost unchanged in the core region. When the Weissenberg number increases, the peak in UHF moves towards the channel center and a noticeable descent in this peak can be observed. In comparison to that of UHF, the wall-normal turbulent heat flux of CTD is larger and reaches a maximum further away from the wall owing to the production caused by the mean temperature gradient in the core region. It is interesting to note that the peak value of $-\overline{v'^{+}\theta'^{+}}$ in Case 3b is larger than that in Case 3a. This magnitude relation is common with the Reynolds shear stress of $-\overline{u'^{+}v'^{+}}$ (figure not shown). It reveals that, irrespective of $DR\%$ and

$HTR\%$, the turbulent heat and momentum transfers are mainly affected by the Weissenberg number: the increase in $HTR\%$ from Case 3a to Case 3b may be caused by a decrease of the conductive sublayer due to the lower effective viscosity.

As mentioned above, the turbulent heat flux is reduced for high Weissenberg-number flows, although the temperature variance is increased as shown in Figure 6. It can thus be conjectured that the turbulent heat flux of $-\overline{v'\theta'}$ should be influenced by the loss of correlation between the two variables, in addition to the decrease of v'. To confirm the decorrelation, the cross-correlation coefficient

$$R_{v\theta} = \frac{-\overline{v'\theta'}}{v'_{\mathrm{rms}}\theta'_{\mathrm{rms}}} \tag{22}$$

was calculated and is depicted in Figure 8. The correlation between v' and θ' in the viscoelastic flow is actually decreased throughout the channel. The maximum value at around $y^+ = 10$ apparently decreased in a similar trend to the wall-normal turbulent heat flux. These trends agree well with those of experimental study by Li and Kawaguchi (2004). Far from the wall, $R_{v\theta}$ decreases significantly for high-$HTR\%$ cases and collapses into a single profile.

3.6. Budget terms of temperature variance

In this section, we consider the budget of the transport equation for the temperature variance in each thermal boundary condition. Here, the transport equation for $\overline{\theta'\theta'}$ for a plane channel flow is

$$\frac{D\overline{\theta'^+\theta'^+}}{Dt^+} = P_\theta - \varepsilon_\theta + T_\theta + D_\theta. \tag{23}$$

Each term on the right-hand side of this equation is as shown below.

$$\text{production:} \qquad P_\theta = -\overline{u_k'^+\theta'^+}\frac{\partial\overline{T^+}}{\partial x_k^+} \tag{24}$$

$$\text{dissipation:} \qquad \varepsilon_\theta = \frac{1}{Pr}\overline{\frac{\partial\theta'^+}{\partial x_k^+}\frac{\partial\theta'^+}{\partial x_k^+}} \tag{25}$$

$$\text{turbulent transport:} \qquad T_\theta = -\frac{1}{2}\frac{\partial}{\partial x_k^+}\overline{u_k'^+\theta'^+\theta'^+} \tag{26}$$

$$\text{molecular diffusion:} \qquad D_\theta = \frac{1}{Pr}\frac{\partial^2}{\partial {x_k^+}^2}\frac{\overline{\theta'^+\theta'^+}}{2} \tag{27}$$

Figure 9 shows the budget terms of temperature variance for UHF as a function of dimensionless wall distance y^+, where the production is plotted in (a), the dissipation in (b), turbulent transport in (c), and the molecular diffusion in (d). The DNS data from Kozuka et al. (2009) are also shown in Figure 9. The maximum value of the residual is less than 2×10^{-2} in all cases. Good balances are achieved, which demonstrates high accuracy in the present DNS.

The peak of the production term for the viscoelastic flow moves to the channel center compared with that in the Newtonian flow (see Figure 9(a)). The moving distance of the peak becomes larger for higher We_τ. For example, Cases 3a and 3b have almost the same location of the peak (at $y^+ \approx 16$) because of the same We_τ, and Case 4 with the highest $DR\%$ and $HTR\%$, achieved in the present study, reveals the peak at $y^+ \approx 18$. With increased the distance of the peak location from the wall, the peak value of P_θ gradually decreases. However, in the outer layer, the production for the viscoelastic flow becomes large as the Weissenberg number increases. This corresponds to the temperature variance of the viscoelastic flow being larger than that of the Newtonian flow in Figure 6. In the vicinity of the wall ($y^+ < 10$), the turbulent transport of the viscoelastic flow, especially for $We_\tau \geq 30$, is much smaller than that of the Newtonian fluid. With respect to the negative peak in the buffer region, Case 4 has smaller turbulent transport than the other cases. In addition, the near-wall energy-gain region of the viscous diffusion for the viscoelastic flow is found to be extended away from the wall up to $y^+ = 10$, implying that the heat-conductive sublayer is expanded.

Similar tendencies can be found in the results for CTD, which are given in Figure 10. The peak of the production term moves towards the channel center, from $y^+ = 9.6$ for Case 1, to $y^+ = 10.7$ (Case 2), $y^+ = 16.3$ (Case 3a), and $y^+ = 19.0$ (Case 4), as given in Figure 10(a). However, in contrast to UHF, the peak value of P_θ for CTD is constant at 0.5, which is consistent with an analytical solution:

$$P_{\theta\max} = \frac{Pr}{4} \qquad \text{at} \quad -\overline{v'^+\theta'^+} = 0.5. \tag{28}$$

The production term is significantly non-zero even at the channel center, whereas it becomes zero for UHF. It can be clearly seen that the production term of viscoelastic flow is larger than that of Newtonian flow in the outer layer and the secondary peak of production exists at the channel center for all cases. In Case 4, the dissipation term is found to be unchanged throughout

the channel, and hence the Batchelor length scale is expected to be almost constant in the channel. The turbulent transport of the viscoelastic flow is smaller than that of the Newtonian fluid. In Case 4, the secondary peak of production exists at the channel center and the turbulent transport is suppressed there. In this case, the mean temperature gradient at the channel center is pronounced, and it is relatively low in the vicinity of the wall (see Figure 3).

4. Conclusion

We systematically performed direct numerical simulations on the turbulent channel flows of a Newtonian fluid and of four different viscoelastic fluids, using the Giesekus constitutive equation with the heat transfer at a Reynolds number of $Re_{\tau 0} = 150$ and a Prandtl number of $\mathrm{Pr} = 2.0$. Moreover, two different boundary conditions were employed in the temperature field. The relationship between the drag reduction and the heat-transfer reduction was investigated. The budget of the temperature variance was also discussed.

Although high $DR\%$ was achieved by two factors, that is,suppression of the turbulence for a fluid with high Weissenberg-number and decrease of the effective viscosity for a low-β fluid, a difference in the increase of $HTR\%$ by these factors, namely, dissimilarity between velocity and temperature fields, was found. A case with low β gave rise to high $DR\%$ with low $HTR\%$ compared with those obtained with high We_τ. Differences were also found in various statistical data such as the mean temperature profile, the temperature variance, the turbulent heat flux, and the budget of the temperature variance. For instance, in high-We_τ case, the peak of the production shifted more to the channel center, which implied that the heat-conductive sublayer expanded, so the heat transfer was suppressed in that case. On the other hand, the decrease in β, which was equivalent to the reduced effective viscosity, did not yield the turbulence suppression. In such a case, the extension of the conductive sublayer was reduced more than that by increasing We_τ, resulting in a relatively small increase in $HTR\%$. This tendency was observed in different boundary conditions in the temperature field.

Note

This paper is a revised and expanded version of a paper entitled "DNS of a drag-reducing viscoelastic turbulent flow with heat transfer" presented

at Asian Symposium on Computational Heat Transfer and Fluid Flow, Jeju, Korea, Oct. 20-23, 2009.

Acknowledgments

The present computations were performed with the use of supercomputing resources at Cyberscience Center of Tohoku University and at Earth Simulator at the Japan Agency for Marine-Earth Science and Technology. This work was partly conducted in the Research Center for Holistic Computational Science (Holcs). We also gratefully acknowledge the assistance of Mr. Takahiro Ishigami, who was a Master's-course student at Tokyo University of Science.

References

Dean, R.B. (1978) 'Reynolds number dependence of skin friction and other bulk flow variables in two-dimensional rectangular duct flow', *Transactions of ASME, Journal of Fluids Engineering*, Vol. 100, pp. 215–223.

Dimant, Y. and Poreh, M. (1976) 'Heat transfer in flows with drag reduction', *Advances in Heat Transfer*, Vol. 12, Irvine, T.F. and Hartnett, J.P., (Eds.), Academic Press, Inc., New York, pp. 77-113

Dimitropoulos, C.D., Sureshkumar, R., Beris, A.N., and Handler, R.A. (2001) 'Budgets of Reynolds stress, kinetic energy and streamwise enstrophy in viscoelastic turbulent channel flow', *Physics of Fluids*, Vol. 13, pp. 1016–1027.

Fukagata, K., Iwamoto, K., and Kasagi, N. (2002) 'Contribution of Reynolds stress distribution to the skin friction in wall-bounded flows', *Physics of Fluids*, Vol. 14, pp. L43–L76.

Gasljevic, K., Aguilar, G. and Matthys, E. F. (2007) 'Measurement of temperature profiles in turbulent pipe flow of polymer and surfactant drag-reducing solutions', *Physics of Fluids*, Vol. 19, 083105, 18 pp.

Gyr, A., and Bewersdorff, H.-W. (1995) *Drag reduction of turbulent flows by additives*, Kluwer Academic Pub.

Ishigami, T., Tsukahara, T., Kawaguchi, Y., and Yu, B. (2009) 'DNS study on viscoelastic effect in drag-reduced turbulent channel flow', *Proceedings of Sixth International Symposium on Turbulence and Shear Flow Phenomena*, 22–24th June, Seoul, Korea, pp. 359–364.

Jovanović, J., Pashtrapanska, M., Frohnapfel, B., Durst, F., Koskinen, J., and Koskinen, K. (2006) 'On the mechanism responsible for turbulent drag reduction by dilute addition of high polymers: theory, experiments, simulations, and predictions', *Transactions of ASME, Journal of Fluids Engineering*, Vol. 128, pp.118–130.

Kays, W.M. and Crawford, M.E. (1980) *Convective Heat and Mass Transfer*, Second edition, McGraw-Hill, New York.

Kagawa, Y., Yu, B., Kawaguchi, Y., Kawamura, H., and Shiraishi, Y. (2008) 'Turbulent heat transfer of viscoelastic fluid flow accompanied by drag reduction with DNS analysis', *Progress in Computational Fluid Dynamics*, Vol. 8, pp. 477–485.

Kozuka, M., Seki, Y., and Kawamura, H. (2009) 'DNS of turbulent heat transfer in a channel flow with a high spatial resolution', *International Journal of Heat and Fluid Flow*, Vol. 30, pp. 514–524.

Li, F.-C. and Kawaguchi, Y. (2004) 'Investigation on the characteristics of turbulence transport for momentum and heat in a drag-reducing surfactant solution flow', *Physics of Fluid*, Vol. 16, pp. 3281–3295.

Li, F.-C., Kawaguchi, Y. and Hishida, K. (2005) 'Structural analysis of turbulent transport in a heated drag-reducing channel flow with surfactant additives', *International Journal of Heat and Mass Transfer*, Vol. 48, pp. 965–973 .

Lumley, J.L. (1969) 'Drag reduction by additives', *Annual Review of Fluid Mechanics*, Vol. 1, pp. 367–384.

Sureshkumar, R., Beris, A.N., and Handler, R.A. (1997) 'Direct numerical simulation of the turbulent channel flow of a polymer solution', *Physics of Fluids*, Vol. 9, pp. 743–755.

Toms, B.A. (1948) 'Some observations on the flow of linear polymer solutions through straight tubes at large Reynolds numbers', *Proceedings of*

First International Congress on Rheology, North-Holland Publishing Co., Amsterdam, pp. 135–141.

Tsukahara, T., Iwamoto, K., Kawamura, H., and Takeda, T. (2006) 'DNS of heat transfer in transitional channel flow accompanied by a turbulent puff-like structure', *Proceedings of Fifth Turbulence, Heat and Mass Transfer*, 25–29th September, Dubrovnik, Croatia, pp. 193–196.

Tsukahara, T. Ishigami, T. Yu, B., and Kawaguchi, Y., (2011) 'DNS study on viscoelastic effect in drag-reduced turbulent channel flow', *Journal of Turbulence*, in press.

Virk, P.S. (1971) 'An elastic sublayer model for drag reduction by dilute solutions of linear macromolecules', *Journal of Fluid Mechanics*, Vol. 45, pp. 417–440.

White, C.M. and Mungal, M.G. (2008) 'Mechanics and prediction of turbulent drag reduction with polymer additives', *Annual Review of Fluid Mechanics*, Vol. 40, pp. 235–256.

Yu, B. and Kawaguchi, Y. (2004) 'Direct numerical simulation of the viscoelastic drag-reducing flow: a faithful finite-difference method', *Journal of Non-Newtonian Fluid Mech.*, Vol. 116, pp. 431–466.

Yu, B. and Kawaguchi, Y. (2005) 'DNS of fully developed turbulent heat transfer of a viscoelastic drag-reducing flow', *International Journal of Heat and Mass Transfer*, Vol. 48, pp.4569–4578.

Yu, B., Li, F., and Kawaguchi, Y. (2004) 'Numerical and experimental investigation of turbulent characteristics in a drag-reducing flow with surfactant additives', *International Journal of Heat and Fluid Flow*, Vol. 25, pp. 961–974.

Zhu, J. and Rodi, W. (1991) 'A low dispersion and bounded convection scheme', *Computer Methods in Applied Mechanics and Engineering.*, 92 (1991), pp. 87–96.

Table 1: Computational conditions

Case	fluid	We_τ	β
Case 1	Newtonian	0	1.0
Case 2	viscoelastic	10	0.5
Case 3a	viscoelastic	30	0.5
Case 3b	viscoelastic	30	0.3
Case 4	viscoelastic	40	0.5

Table 2: Mean-flow variables including drag and heat-transfer reduction rates

	Bulk Reynolds no.,			*HTR%*		*HTR%/DR%*	
Case	$Re_\mathrm{m} = 2u_\mathrm{m}\delta/\eta_0$	η_eff/η_0	*DR%*	UHF	CTD	UHF	CTD
Case 1	4650	1.000	—	—	—	—	—
Case 2	5140	0.872	21.0%	16.4%	19.3%	0.78	0.92
Case 3a	7900	0.690	62.8%	61.5%	66.7%	0.98	1.06
Case 3b	8860	0.518	69.5%	65.6%	69.9%	0.94	1.01
Case 4	9210	0.654	71.5%	72.8%	77.9%	1.02	1.09

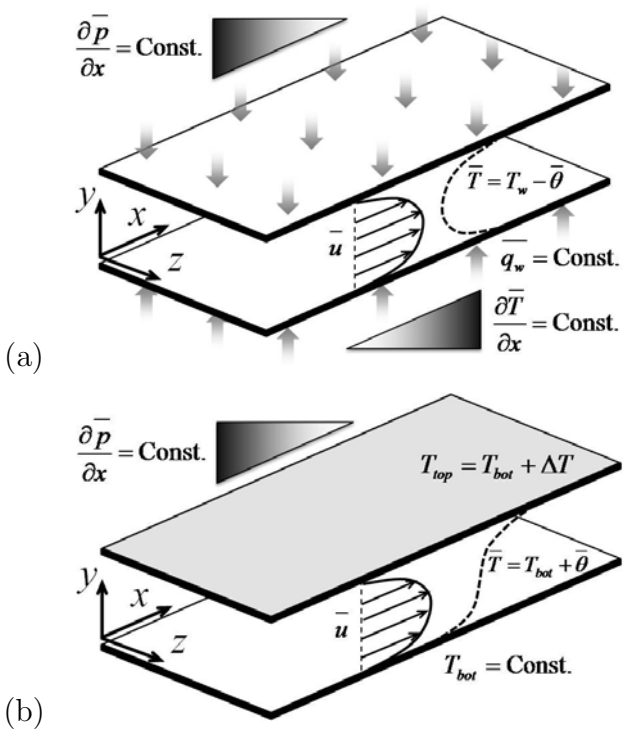

Figure 1: Configuration of a pressure-driven channel flow and thermal boundary conditions: (a) uniform heat-flux heating, UHF; (b) constant temperature difference between two walls, CTD.

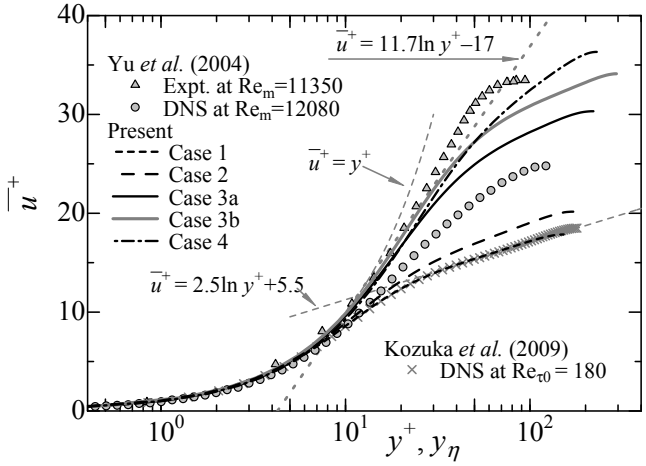

Figure 2: Mean velocity profile in wall unit.

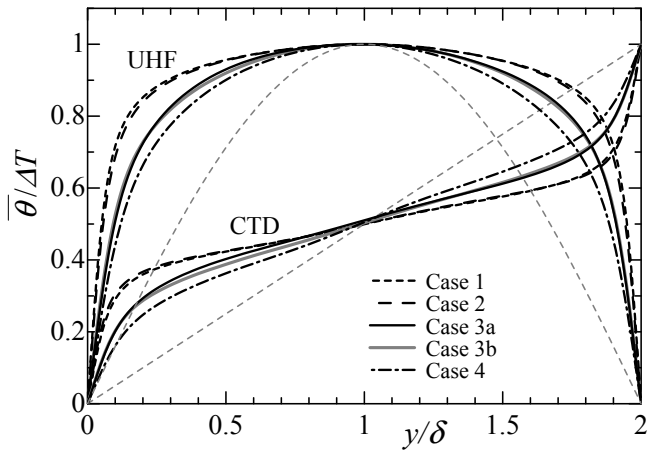

Figure 3: Mean temperature profile normalized by maximum temperature or temperature difference.

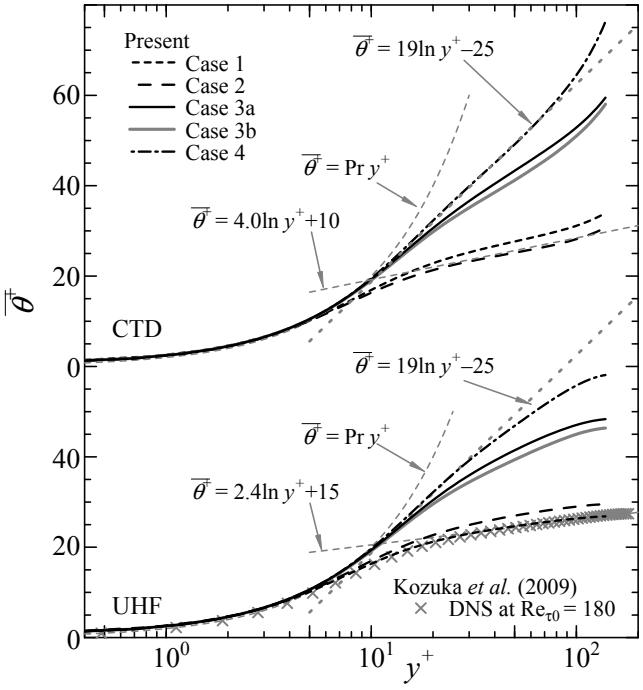

Figure 4: Mean temperature profile in wall unit.

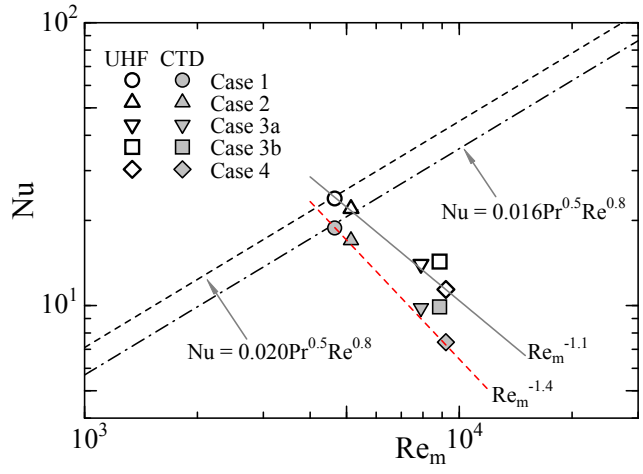

Figure 5: Nusselt number *versus* bulk Reynolds number.

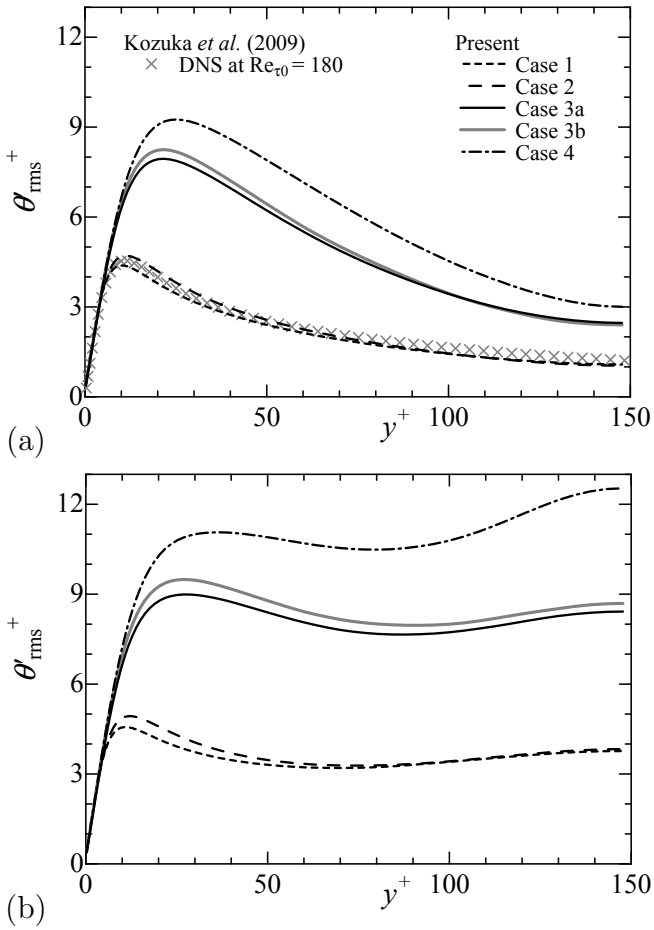

Figure 6: Temperature variance: (a) UHF and (b) CTD.

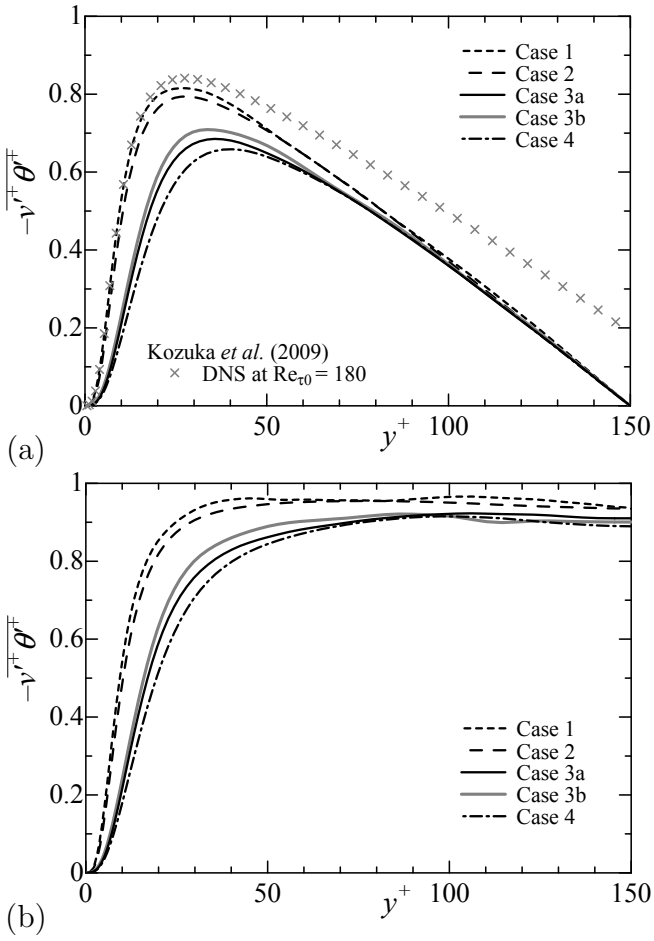

Figure 7: Wall-normal turbulent heat flux: (a) UHF and (b) CTD.

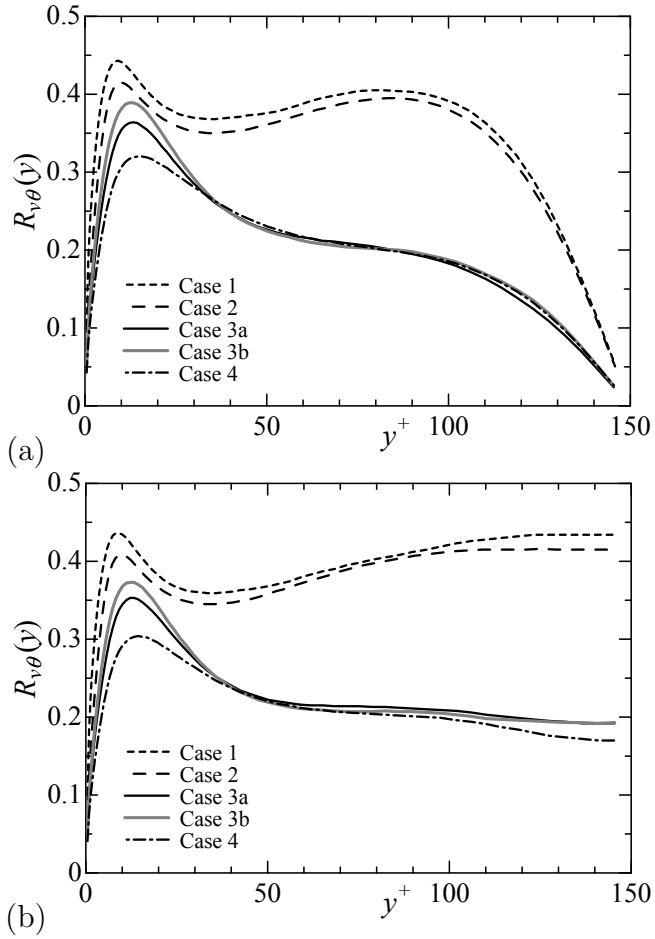

Figure 8: Cross-correlation coefficient between the wall-normal velocity and temperature fluctuations: (a) UHF, (b) CTD.

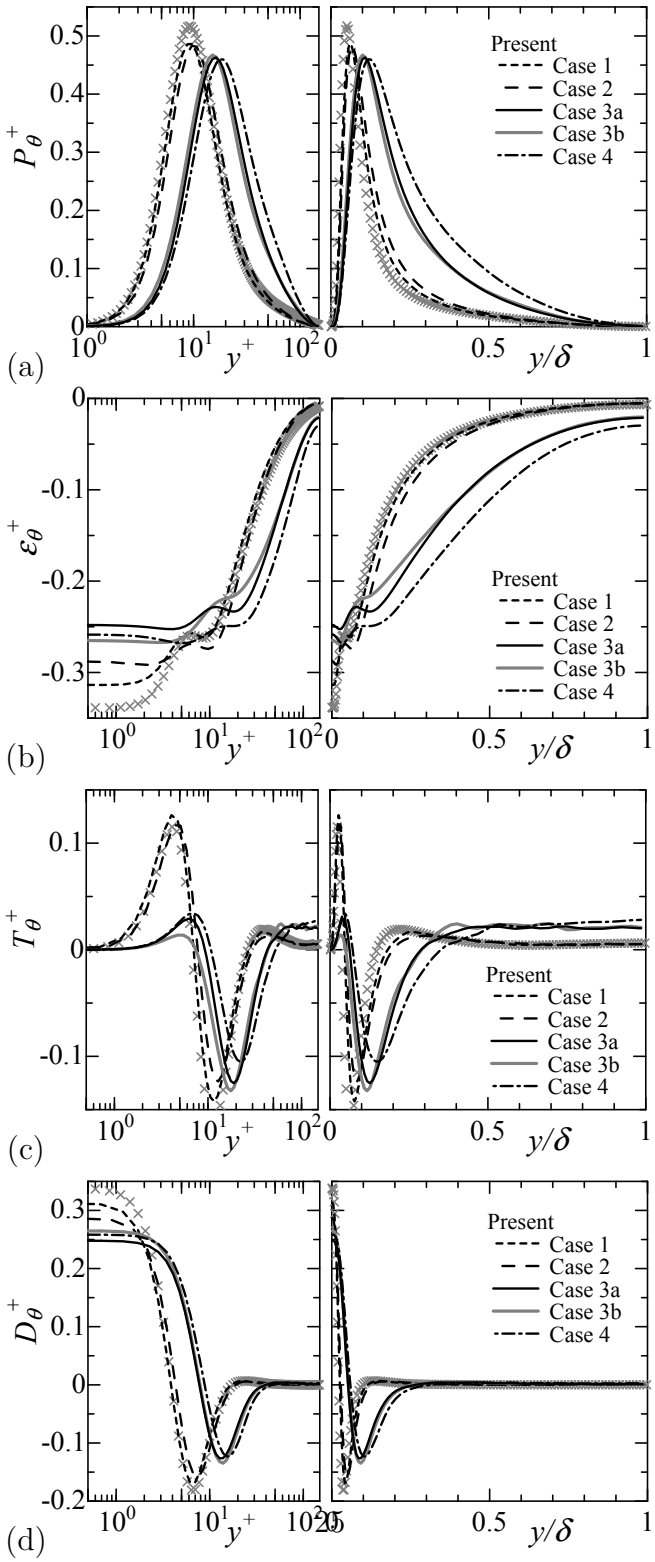

Figure 9: Vertical profiles of terms in temperature variance $\overline{\theta'\theta'}$ budget of Equation (23) for UHF: (a) production, (b) dissipation, (c) turbulent transport, and (d) molecular diffusion. The symbol $\times$ represents the results obtained by Kozuka et al. (2009) for a Newtonian flow at $Re_\tau = 180$ and $Pr = 2$.

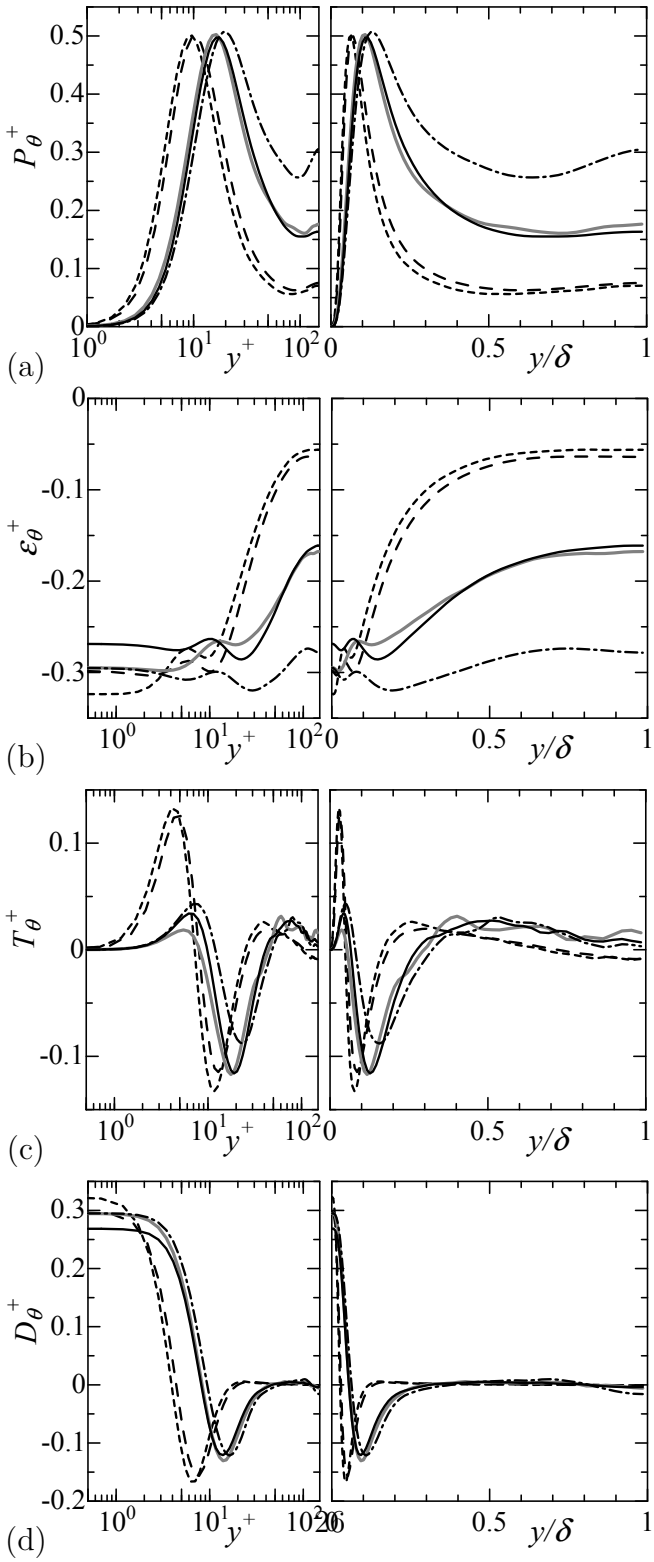

Figure 10: Same as Figure 9 but for CTD.